Journal of Alloys and Compounds 578 (2013) 394–404

Contents lists available at SciVerse ScienceDirect

Journal of Alloys and Compounds

journal homepage: www.elsevier.com/locate/jalcom

Microstructure and mechanical properties of an Al–Mg alloy solidified under high pressures

J.C. Jie [a,b,*], C.M. Zou [b], E. Brosh [c], H.W. Wang [b], Z.J. Wei [b,*], T.J. Li [a]

[a] Laboratory of Special Processing of Raw Materials and School of Material Science and Engineering, Dalian University of Technology, Dalian 116024, China
[b] School of Materials Science and Engineering, Harbin Institute of Technology, Harbin 150001, China
[c] NRCN, P.O. Box 9001, Beer-Sheva 84190, Israel

ARTICLE INFO

Article history:
Received 14 February 2013
Received in revised form 25 April 2013
Accepted 26 April 2013
Available online 6 May 2013

Keywords:
Metals and alloys
Intermetallics
Phase diagrams
Rapid-solidification
Quenching
Microstructure

ABSTRACT

Phase formation, the microstructure and its evolution, and the mechanical properties of an Al–42.2 at.% Mg alloy solidified under high pressures were investigated. After solidification at pressures of 1 GPa and 2 GPa, the main phase is the γ phase, richer in Al than in equilibrium condition. When the pressure is further increased to 3 GPa, the main phase is the supersaturated Al(Mg) solid solution with Mg solubility up to 41.6 at.%. Unlike in similar alloys solidified at ambient pressure, the β phase does not appear. Calculated high-pressure phase diagrams of the Al–Mg system show that although the stability range of the β phase is diminished with pressure, it is still thermodynamically stable at room temperature. Hence, the disappearance of the β phase is interpreted as kinetic suppression, due to the slow diffusion rate at high pressures, which inhibits solid–solid reactions. The Al–42.2 at.% Mg alloy solidified under 3 GPa has remarkably enhanced ultimate tensile strength compared to the alloy solidified under normal atmospheric pressure.

1. Introduction

Al–Mg alloys have been widely used in wrought and cast conditions due to their corrosion resistance, mechanical properties, low density, and formability. In the equilibrium Al–Mg phase diagram, the β-Al_3Mg_2 phase (space group $Fd\bar{3}m$) is a stable intermetallic compound with a large unit cell containing 1168 atoms [1]. The γ-$Al_{12}Mg_{17}$ phase (space group $I4\bar{3}m$) also has a cubic structure but with a much smaller unit cell containing 58 atoms [2]. Both intermetallics are very brittle, which is detrimental to the mechanical properties of Al–Mg alloys [3].

Matsumuro et al. [4] used processing at high pressure of 5.4 GPa to achieve significant improvement in the properties of Mg-rich Al–Mg alloys. The key phenomenon responsible for the alteration of mechanical properties in the experiment of Matsumuro et al. [4] was the increase in the solubility of Al in HCP-Mg with applied pressure.

A similar increase in solubility was observed by Minamino et al. [5] in their high pressure diffusion-couple experiments on the Al-rich side of the Al–Mg system. This indicates a possibility that high pressure processing can also result in improved mechanical properties in Al-rich Al–Mg alloys.

The purpose of this work is to study phase formation, microstructure evolution, and properties of an Al–Mg alloy produced by solidification under high pressures. The experimental work is accompanied by thermodynamic modeling of the Al–Mg system, extended to high pressure.

2. Experimental

An Al–Mg alloy with 42.2 at.% Mg was prepared by conventional casting from 99.99 wt.% pure Al and Mg. The samples for high pressure solidification were cylinders 20 mm in diameter and 18 mm in length; details of high pressure solidification are described elsewhere [6]. The phases were characterized by a Rigaku D/max-RB X-ray diffractometer with monochromatic Cu Kα radiation. The step size and step time were 0.02° and 1 s per step, respectively. Morphology was examined on an Olympus optical microscope and a scanning electron microscope (SEM) operated at 20 kV equipped with an energy dispersive X-ray spectrometer (EDX). Fractographic analysis was performed on a scanning electron microscope (S4700). Tensile tests were carried out using an INSTRON 5569 testing machine at a strain rate of 10^{-3} s^{-1}. All of the samples were cut into dog-bone-shaped specimens with gauge length of 13.0 mm and cross-section of 1.5 mm × 1.0 mm for tensile tests [7]. In order to examine reproducibility, five replicates were used.

3. Results

3.1. Microstructure

The microstructures of Al–42.2 Mg alloy solidified under different pressures are shown in Fig. 1 and the corresponding X-ray

* Corresponding authors. Address: Laboratory of Special Processing of Raw Materials and School of Material Science and Engineering, Dalian University of Technology, Dalian 116024, China. Tel./fax: +86 411 84708940 (J.C. Jie), tel.: +86 451 86403150 (Z.J. Wei).
E-mail addresses: jiejc@dlut.edu.cn (J.C. Jie), weizj@hit.edu.cn (Z.J. Wei).

0925-8388/$ - see front matter © 2013 Elsevier B.V. All rights reserved.
http://dx.doi.org/10.1016/j.jallcom.2013.04.184

diffractions (XRDs) are shown in Fig. 2. It can be seen that the Al–42.2 Mg alloy solidified under normal atmospheric pressure contains the β and γ phases (Fig. 1a1). Eutectic colonies composed of the lamellar β and γ phases are distributed in the β matrix (Fig. 1a2). When the pressure is 1 GPa, the matrix is the γ phase with dotted FCC-Al(Mg) solid solution (FCC) and eutectic γ phases distributed in the inter-dendritic region (Fig. 1b1 and b2). The amount of α-Al increases, and the γ phase together with the dotted FCC (Fig. 1c1) are formed in the inter-dendritic region when the pressure increases to 2 GPa. The eutectic colonies composed of the FCC and γ phases are also formed in the inter-dendritic region (Fig. 1c1 and c2). A small amount of lamellar eutectic structure (Fig. 1d2) distributes in the supersaturated FCC matrix under 3 GPa (Fig. 1d1).

It can be seen that the microstructure of Al–42.2 at.% Mg alloy is strongly influenced by the solidification pressure. Notably, the β intermetallic, which is prominent in the ambient-pressure solidified alloy, is absent when the solidification is performed at high pressure.

3.2. Mg solubility in FCC

The Mg content in the FCC phase in the solidified structures was determined by EDX. In the Al–42.2 at.% Mg alloy solidified under 2 GPa and 3 GPa, the measured Mg-content in the FCC, measured by EDX, was 37.1 at.% and 41.2 at.%, respectively (see Fig. 3). These measured values are much higher than the equilibrium solubility of 17 at.% Mg in Al at the eutectic temperature and ambient pressure.

The Mg content of the FCC was also estimated from the lattice parameters as measured by XRD. The lattice parameters of FCC solidified under 2 GPa and 3 GPa can be calculated from the XRD

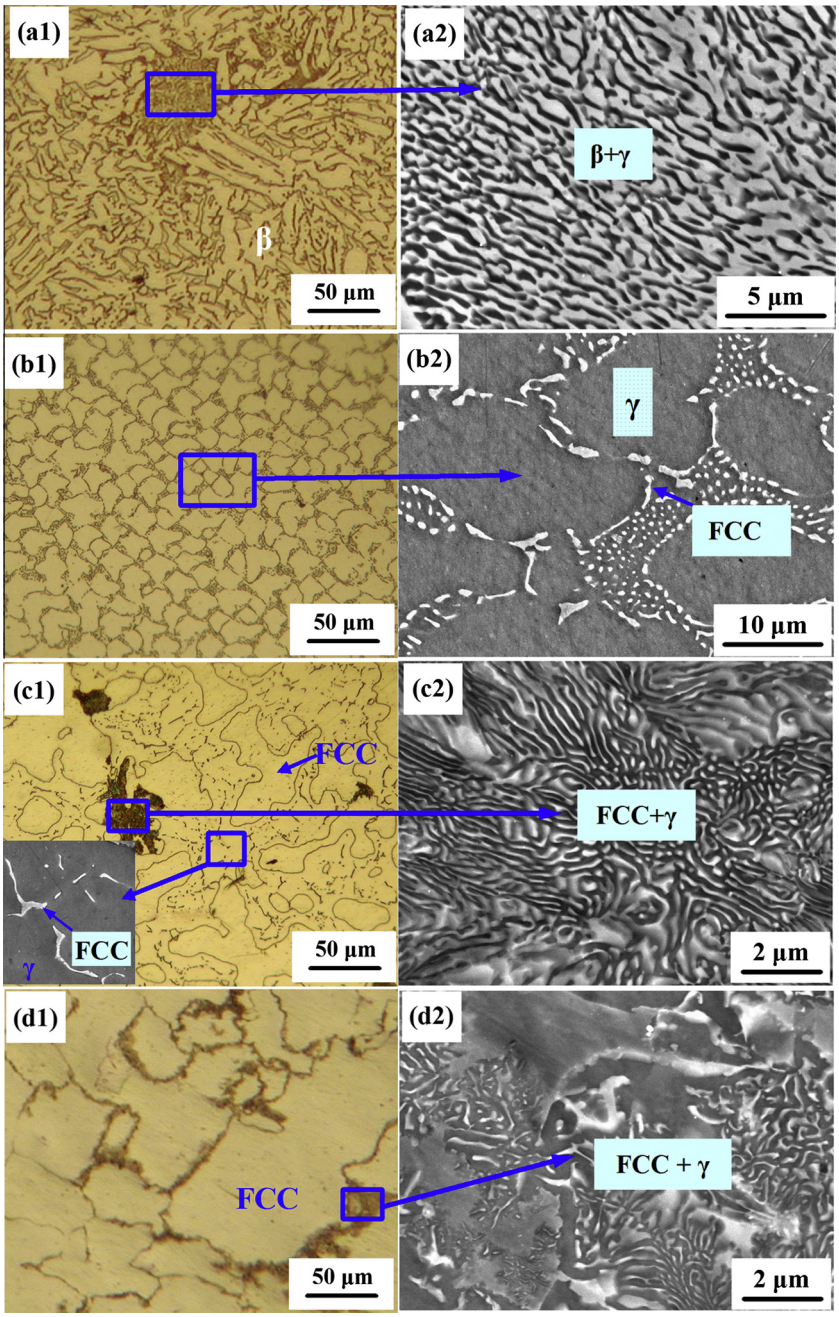

Fig. 1. Microstructures of Al–42.2Mg alloy solidified under different pressures. (a) Normal atmospheric pressure, (b) 1 GPa, (c) 2 GPa, and (d) 3 GPa.

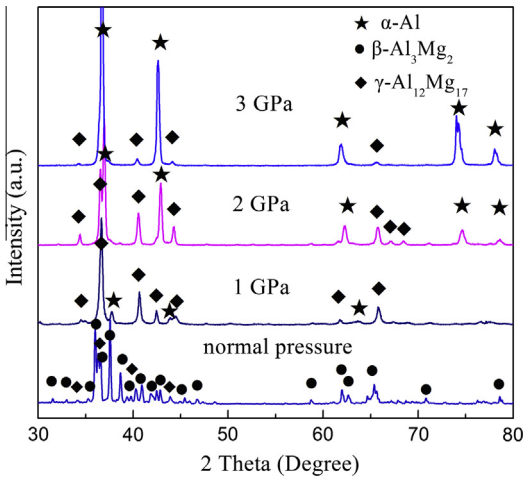

Fig. 2. XRD patterns of Al–42.2Mg alloy solidified under different pressures.

patterns, which are 0.4215 ± 0.0001 nm and 0.4235 ± 0.0001 nm, respectively. The lattice parameter of the FCC under 1 GPa could not be calculated as there are fewer reflections of FCC.

Determination of the Mg-content of the FCC phase by interpretation of the lattice parameter data requires the use of empirical correlations between the lattice parameters and the composition, developed from supersaturated FCC Al–Mg alloys. Such alloys were prepared by various methods, such as rapid solidification (RS) [8], mechanical milling (MM) of pre-alloyed Al–Mg ingots [9], and mechanical alloying (MA) [10,11].

The solubility of Mg in the FCC as measured by EDX and as estimated from our XRD lattice parameter measurements using various empirical correlations is shown in Table 1. It can be seen that the EDX results are in excellent agreement with the correlation developed from alloys prepared by rapid solidification but not with correlations based on alloys prepared by MM or MA. Indeed, the process of rapid solidification (RS) is more similar to the present experiment than MM and MA and probably produces similar defects in the crystal structure.

3.3. Composition of the γ phase

The XRD patterns of samples solidified under different pressures, including the reflections from the γ phase, are presented in Fig. 4a. It can be seen that the reflections from the γ phase solidified at ambient pressure are close to their standard position [12] (highlighted as blue[1] lines). This corresponds to a Mg-content of around 59 at.% Mg, the equilibrium concentration of the γ phase at room temperature. In the alloy solidified at 1 GPa the reflections shift to the right, indicating that the lattice parameter of the γ phase decreases. For the alloys solidified at a pressure of 2 GPa, the reflections move back to the left. Since the lattice parameter of the gamma phase is positively correlated with its Mg content [13], the XRD results indicate that the Mg-content of the γ phase in samples solidified under high pressures is lower than that solidified under ambient pressure, but further increase of pressure increases the Mg-content.

The compositions of the γ phase in the samples solidified under 1 GPa and 2 GPa were measured by EDX and found to be 44.9 at.% and 48.2 at.% (Fig. 4b and c), respectively. Both of these values are significantly lower than the 59 at.% concentration determined from XRD[2] in the alloy solidified at ambient pressure.

[1] For interpretation of color in Fig. 4, the reader is referred to the web version of this article.

[2] The Mg-content of the γ phase in the alloy solidified at ambient pressure could not be measured by EDX because of its fine lamellar microstructure.

The XRD and EDX measurements of the composition of the γ phase are summarized in Table 2, where reasonable agreement between the two analytical methods can be seen.

It should be noted that the Mg composition in the γ phase is not constant due to the segregation during solidification. The width of the γ phase solidified under 3 GPa is only about 0.1–0.2 μm (see Fig. 2d2). Thus, the Mg composition cannot be accurately measured due to the larger diameter of the electron beam of about 2 μm. However, it can still be deduced that the Mg content of the γ phase solidified under 3 GPa is greater than that under 2 GPa.

3.4. Phase content

Fig. 2 presents the X-ray diffraction patterns of Al–42.2 at.% Mg alloy solidified under different pressures. The Al–42.2 at.% Mg alloy solidified under normal atmospheric pressure contains the β and γ phases. When the pressure is 1 GPa, the peaks of the β phase disappear, replaced by the intense reflections of the γ phase and a few tiny reflections of FCC-Al solid solution with dissolved Mg in FCC. When the pressure is increased to 2 GPa the reflections of FCC increase; meanwhile, the reflections of the γ phase decrease. When the pressure is increased to 3 GPa the XRD pattern mainly contains the reflections of FCC and several tiny reflections of the γ phase. Hence, the fraction of the FCC phase increases with increasing pressure.

Due to the small specimen size and the complexity of the diffraction patterns, we were unable to use overall fitting of the XRD patterns for quantitative determination of the phase content in the solidified alloys. Instead, the phase fractions were calculated from the lever rule, assuming only two phases: FCC and γ:

$$c_\gamma = \frac{x^0_{Mg} - x^{FCC}_{Mg}}{x^\gamma_{Mg} - x^{FCC}_{Mg}} \quad (1)$$

where x^0_{Mg} is the overall fraction of Mg in the alloy (42.2%), and x^{FCC}_{Mg} and x^γ_{Mg} correspond to the compositions of the FCC and γ phases, respectively, determined from the measured lattice parameters, as given in Tables 1 and 2. For the sample solidified at ambient pressure, the calculation was performed for β and γ phases with $x^\beta_{Mg} = 0.3885$. The results of these estimations are shown in Table 3.

3.5. Mechanical properties

In order to investigate the effects of high pressure solidification on mechanical properties of Al–42.2 at.% Mg alloy, tensile tests of samples solidified under normal atmospheric pressure and 3 GPa were conducted. The Al–42.2 at.% Mg alloy solidified under 3 GPa has an ultimate tensile strength (UTS) of 95.8 ± 7.3 MPa, while the sample solidified under normal atmospheric pressure has a UTS of 8.6 ± 3.1 MPa, suggesting that the tensile strength is greatly improved by solidification under high pressure. But the two alloys solidified under different pressures have small elongations of less than 0.2%, resulting in our inability to measure the yield stress. Fig. 5 shows the fracture surfaces of Al–42.2 at.% Mg alloy solidified under normal atmospheric pressure and 3 GPa. Both samples exhibit a brittle transgranular fracture, resulting in the small elongations. In particular, the FCC solid solution with high Mg solubility exhibits obvious cleavage fracture characteristics, due to the existence of plateaus and edges as highlighted in the dotted blue line.

4. Thermodynamic modeling

We performed calculations of high pressure phase equilibria of the Al–Mg system using the Thermo-calc software [14]. While a thermodynamic calculation of the Al-rich part of the Al–Mg system at high pressures was done in the past by Minamino et al. [5], in

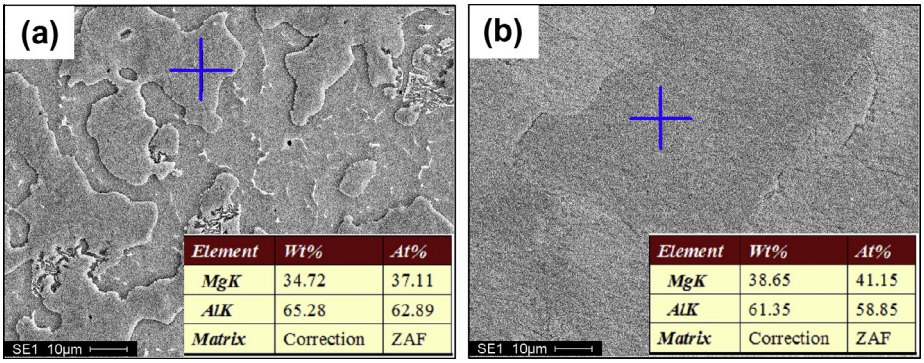

Fig. 3. EDX results of Al(Mg) solid solution in the Al–42.2Mg alloy solidified under different pressures: (a) 2 GPa, and (b) 3 GPa.

Table 1
Mg contents in the FCC phase of Al–42.2Mg alloy solidified under different pressures.

Pressure (GPa)	Lattice parameter (nm)	Mg-content in FCC (at.%)						
		From lattice parameter			EDX	Minamino T = 733 K	Thermodynamic calculation	
		RS [8][a]	MA [11][b]	MM [30][c]			Equilibrium for T = 733 K	At solidus temperature
1	0.4125 ± 0.0003	17 ± 1	–	–	–	–	–	23.2
2	0.4215 ± 0.0001	37 ± 1	~41	~64	37.1	25.8	26.3	29.7
3	0.4235 ± 0.0001	42 ± 1	~45	~67	41.2	32.7	30.1	37.2

[a] The correlation was developed based on RS alloys.
[b] The correlation was developed based on MA alloys.
[c] The correlation was developed based on MM alloys.

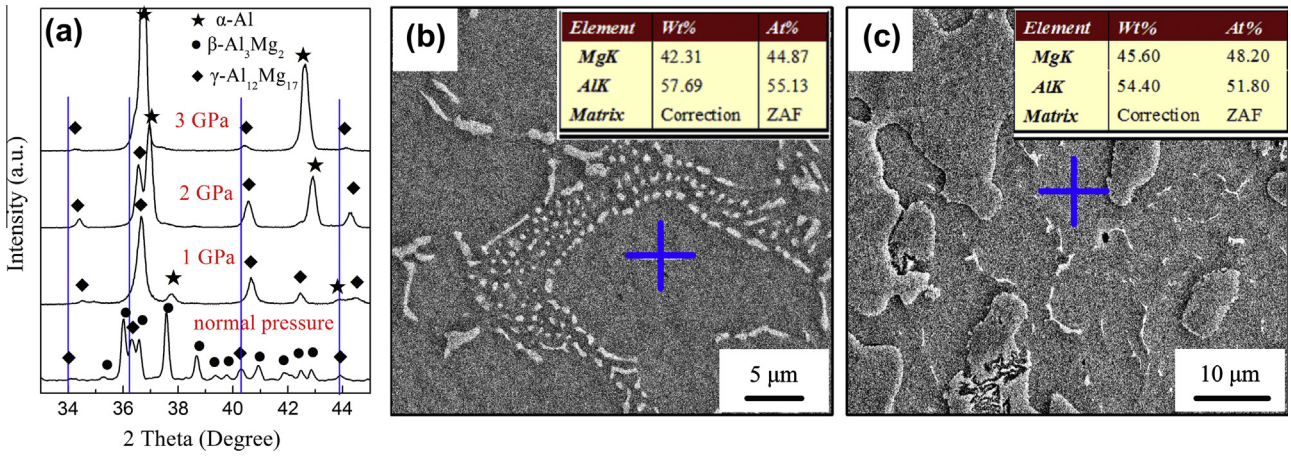

Fig. 4. (a) Reflections of the γ phase under different pressures. The blue line represents the standard peaks of the equilibrium γ-$Al_{12}Mg_{17}$ phase. EDX of the γ phase in the sample solidified under (b) 1 GPa and (c) 2 GPa.

the present work we attempt a more comprehensive and more precise model, taking into account up-to-date experimental and theoretical information.

Calculation of the Al–Mg phase diagram in the present work is based on a CALPHADs (Calculation of Phase Diagrams) thermodynamic model [15]. The Gibbs energy of each phase as a function of temperature, composition, and pressure is modeled by a semi-empirical mathematical expression over the widest possible range of the aforementioned variables. The expressions for the Gibbs free energy contain adjustable parameters that are fitted to various experimental data, including calorimetric information, thermophysical properties, and phase equilibria. Theoretical calculations may also be used for constraining model parameters. For example, Zhong et al. [16] used ab initio calculations to calibrate their model of the Al–Mg system at ambient pressure.

In the present work, the model of Zhong et al. [16], which gives the Gibbs energy of each phase as a function of temperature T and composition x at ambient pressure P_0, was extended to high pressure by:

$$G(T,P,x) = G(T,P_0,x) + \int_{P_0}^{P} V(T,P',x)\,dP' \quad (2)$$

where $V(T, P', x)$ is a composition-dependent semi-empirical EOS (Equation Of State), described in the Appendix. As customary in CALPHAD modeling, the EOS contains adjustable parameters that need to be fitted to calibrate the model. The types of data used for calibration of the EOS were thermophysical properties (listed in Table 4) and determinations of phase equilibria. Of the latter type, two sources exist in the literature: Minamino et al. [5], who

Table 2
The Mg-content of the γ phase, measured by XRD and EDX compared to the results of thermodynamic calculations.

P	Lattice parameter (nm)	Mg content in γ (at.%)			
		Determined from lattice parameter	EDX As solidified	Calculated equilibrium at solidus	Calculated equilibrium at *T* = 300 K
Normal pressure	1.0578 ± 0.0005	59 ± 1	–	47.42	57.6
1 GPa	1.0410 ± 0.0002	45 ± 1	44.87	48.3	57.7
2 GPa	1.0442 ± 0.0001	48 ± 1	48.20	50.8	57.8
3 GPa	1.05 ± 0.005	~58	–	53	57.9

Table 3
Phase content of an Al–42.2 at.% Mg solidified at high pressures.

P	Experimental	Thermodynamic calculation			
		Calculated equilibrium at *T* = 300 K	Equilibrium at solidus temperature	Scheil model	Partitionless (β suspended)
Normal pressure	FCC: 0% γ: 16% β: 84%	FCC: 0% γ: 18% β: 82%	FCC: 0% γ: 39% β: 61%	FCC: 0% γ:32% β: 68%	FCC: 0% γ: 100%
1 GPa	FCC: 10% γ: 90%	FCC: 0% γ: 18% β: 82%	FCC: 24% γ: 76%	FCC: 24% γ: 76%	FCC: 0% γ: 100%
2 GPa	FCC: 47% γ: 53%	FCC: 0% γ: 18% β: 82%	FCC: 41% γ: 59%	FCC: 40% γ: 60%	FCC: 0% γ: 100%
3 GPa	FCC: 99% γ: 1%	FCC: 0% γ: 18% β: 82%	FCC: 68% γ: 32%	FCC: 55% γ: 45%	FCC: 100% γ: 0%

conducted high-pressure Al/Mg diffusion couple experiments, and Matsumuro et al. [4], who performed high-pressure quenching experiments on Mg-rich Al–Mg alloys. These data are not entirely consistent. The results of Matsumuro et al. indicate that the eutectic temperature on the Mg-rich side is below 773 K at *P* = 5.4 GPa, while Minamino et al. did not detect melting at 793 K at a much lower pressure of 2.2 GPa. Since melting temperatures should rise with pressure, this discrepancy of melting temperatures is actually larger than just the apparent 20°. Data on thermophysical properties pose additional constraints on the selection of EOS parameters. Hence the selected parameters represent a compromise between the various data.

The available data on the molar volume of the liquid and solid phases are shown in Fig. 6a, together with the corresponding calculations. It is seen in Fig. 6a that the molar volume of solid solution phases, as well as of intermetallic compounds, is reproduced by the fitted EOS. The present calculation also reproduces the experimentally observed negative deviation of the liquid molar volume from an ideal mixing rule, although the calculated deviation is smaller than that measured. This is different from the previous model by Minamino et al. [5], which is also shown in Fig. 6a. It is clear that the values of the liquid molar volume used by Minamino et al. are too high and indeed such values of the liquid molar volume will be needed in order to reproduce the high eutectic temperature they indicated.

The bulk moduli of the FCC and HCP solid solutions are shown in Fig. 6b, and the sound velocity in liquid Al–Mg alloys is shown in Fig. 6c. It is seen that these parameters are reasonably well reproduced by the model. Also, the properties of the β phase are well fit by the model, as shown in Fig. 6d and e.

After the adjustable parameters of the model were fitted, i.e., the model was calibrated, it is possible to use it for consistent calculations of phase equilibria and thermodynamic properties at various pressures, temperatures, and compositions. Calculated phase diagrams for several pressures are shown in Fig. 7a–e, together with the corresponding experimental results by Minamino et al. [5] and Matsumuro et al. [4]. The results of Minamino et al. are reasonably reproduced by the model, except that the calculated melting temperature at 2.2 GPa is too low. Indeed the higher melting point indicated by Minamino et al. could be reproduced only if the molar volume of the liquid was taken to be significantly larger. On the other hand, the model did not fit the low melting temperature detected by Matsumuro et al. at 5.4 GPa, the reproduction of which would require the selection of a lower molar volume for the liquid.

4.1. Model calculation results

The calculated phase diagrams shown in Fig. 7a–e are characterized by increased solubility of Mg in Al (FCC) with the increase of pressure, as previously discovered by Minamino et al. [5]. The calculated concentration of Mg in FCC in comparison with the experimental results is shown in Table 1 and Fig. 7f. Two calculations are given in the table: a calculation as a function of pressure at a fixed temperature of *T* = 733 K, to enable comparison with Minamino et al. [5]; and a calculation for each pressure that is done at the solidus temperature of the Al–42.2 at.% Mg alloy. The results of both calculations are quite close and in good agreement with Minamino et al. [5]. The experimental results of the present work indicate a much higher concentration of Mg in the FCC phase than both Minamino et al. and the preset thermodynamic calculation.

The composition of the γ phase, calculated at *T* = 300 K and at the solidus temperature of the alloy, is given in Table 2. At ambient pressure, the solidus equilibrium calculation gives a significantly lower value than the experimental one. This does not indicate that the calculation is inaccurate since it does reproduce the experimental ambient-pressure phase diagram. Rather, it seems that at ambient pressure, the diffusion is fast enough to reach equilibrium even at low temperatures; hence the 300 K calculation is closer to the experimental result at ambient pressure. At higher pressures, the calculation reproduces the experimentally observed tendency of increase in the Mg content in the γ phase, as seen in Table 2 and shown graphically in Fig. 7f.

The calculated phase content is shown in Table 3. The calculation was done under four alternative assumptions:

- An equilibrium calculation at 300 K, assuming that the diffusion is fast enough to establish equilibrium, down to room temperature.

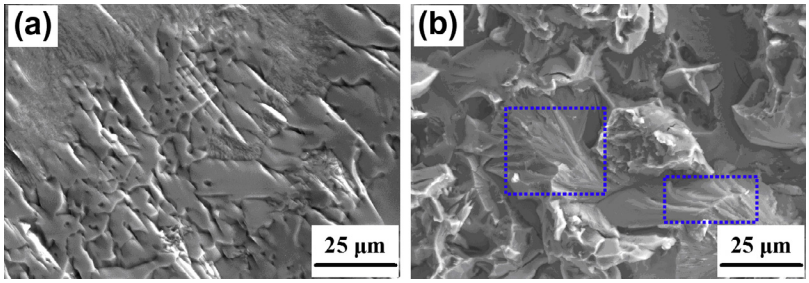

Fig. 5. Fractographs of the tensile samples solidified under normal atmospheric pressure and 3 GPa. (a) Normal pressure, and (b) 3 GPa. The dotted blue frame indicates the cleavage fracture characteristic of Al(Mg) solid solution. (For interpretation of the references to color in this figure legend, the reader is referred to the web version of this article.)

- An equilibrium calculation at the solidus temperature. This corresponds to a very sharp temperature dependence of diffusion: assuming that diffusion is fast enough to reach equilibrium above the solidus in both liquid and solid but with no diffusion below the solidus.
- A Scheil–Gulliver simulation [15], under the assumption that at the conditions of the experiment, the diffusion in the liquid phase can be considered to be infinitely rapid, while that in the solid is considered to be infinitely slow.
- A "partitionless" calculation, conducted as if the phase transformation from liquid to FCC or γ occurs at a single temperature, and the composition of all participant phases is the same as the overall composition of the alloy. This assumption may be valid if the rate of cooling is so fast that the diffusion in both liquid and solid phases may be considered to be infinitely slow.

Certainly, the actual solidification process cannot be captured by any one of these simplifying assumptions. Nevertheless, it is reasonable to envisage the real process as lying somewhere between such limiting cases. One can see in Table 3 that the experimentally observed tendency of moving from a predominantly γ microstructure at 1 GPa to a predominantly FCC microstructure at 3 GPa is reproduced by the calculation under all assumptions, except for the 300 K equilibrium. Moreover, it can be seen in Fig. 7b that the first solidified phase (for Al–42.2 at.% Mg) is γ whereas the primary phase at higher pressures is FCC, in agreement with the observed microstructure.

At ambient pressure, the calculation that fits the experimental results most accurately is the 300 K equilibrium calculation. At 1 and 2 GPa both Scheil and solidus calculations give FCC and γ phases, not too far from the experimental phase content determination. The partitionless calculation is obviously erroneous at these pressures. However, at a pressure of 3 GPa the partitionless calculation is closest to the experimental results.

Above ambient pressure, none of the calculations result in β phase in the solidified structure. However, although the stability range of the β phase is diminished with an increase of pressure, it is predicted to be thermodynamically stable up to around 5.4 GPa. If the enough time is given, β may still form by a solid–solid reaction.

It should be noted that while this main prediction is fairly robust, the quantitative details depend on the particular choice of model parameters; for example, changing the ambient-pressure model to the results of Liang et al. [17] in a prediction that the β phase ceases to be stable around $P = 2.7$ GPa instead of $P = 5.4$ GPa as predicted with the present model (based on Zhong et al. [16]). Also, it should be noted that the current thermodynamic model treats β phase as a stoichiometric compound, while it is known to have some finite composition range [13].

5. Discussion

5.1. Microstructure

The thermodynamic model is in agreement with the experimental results on several aspects of the microstructural evolution in the Al–42.2 at.% Mg alloy during high pressure solidification:

a. The solubility of Mg in the FCC phase increases with the increase of pressure.
b. The concentration of Mg in the gamma phase increases with the increase of pressure from 1 GPa to 3 GPa.
c. The increase of pressure causes an increase in the fraction of FCC at the expense of γ phase.

However, according to the calculation, the β phase is predicted to be stable and is expected be formed through a peritectoid reaction of α + γ → β. In addition, the β phase did form in the Al–12Mg and Al–21.6Mg alloys solidified under 1 GPa in our previous work [6,18]. However, it is known that the β phase can be suppressed by very rapid cooling [19].

We suggest that the reason for the absence of β phase in the present work is the slowing down of diffusion at high pressure. The diffusion coefficient of Mg in Al decreases with increasing

Table 4
Data sources for thermophysical properties for calibration of the EOS for pure Mg and Al–Mg alloys.

Phase/composition	Ambient pressure molar volume	Ambient pressure thermal expansion	Compressibility
HCP: pure Mg	[31]	[31]	[32,33]
Liquid: pure Mg	[34]	[34]	[35]
FCC: Al–Mg	[36]	[37][a]	[38]
HCP: Al–Mg	[36]	–	[4]
β	[13,39]	[39]	[39]
γ	[40]	[41][b]	[42][b]
ε	[13,42]	–	[42][b]
Liquid: Al–Mg	[43–45]	–	[35]

[a] This experiment by Gasior et al. [37] proved to be difficult to reconcile with data given by Hallstedt [36], which we judge to be more reliable.
[b] Ab initio calculations that were given lighter weight in the calibration, compared to experimental data.

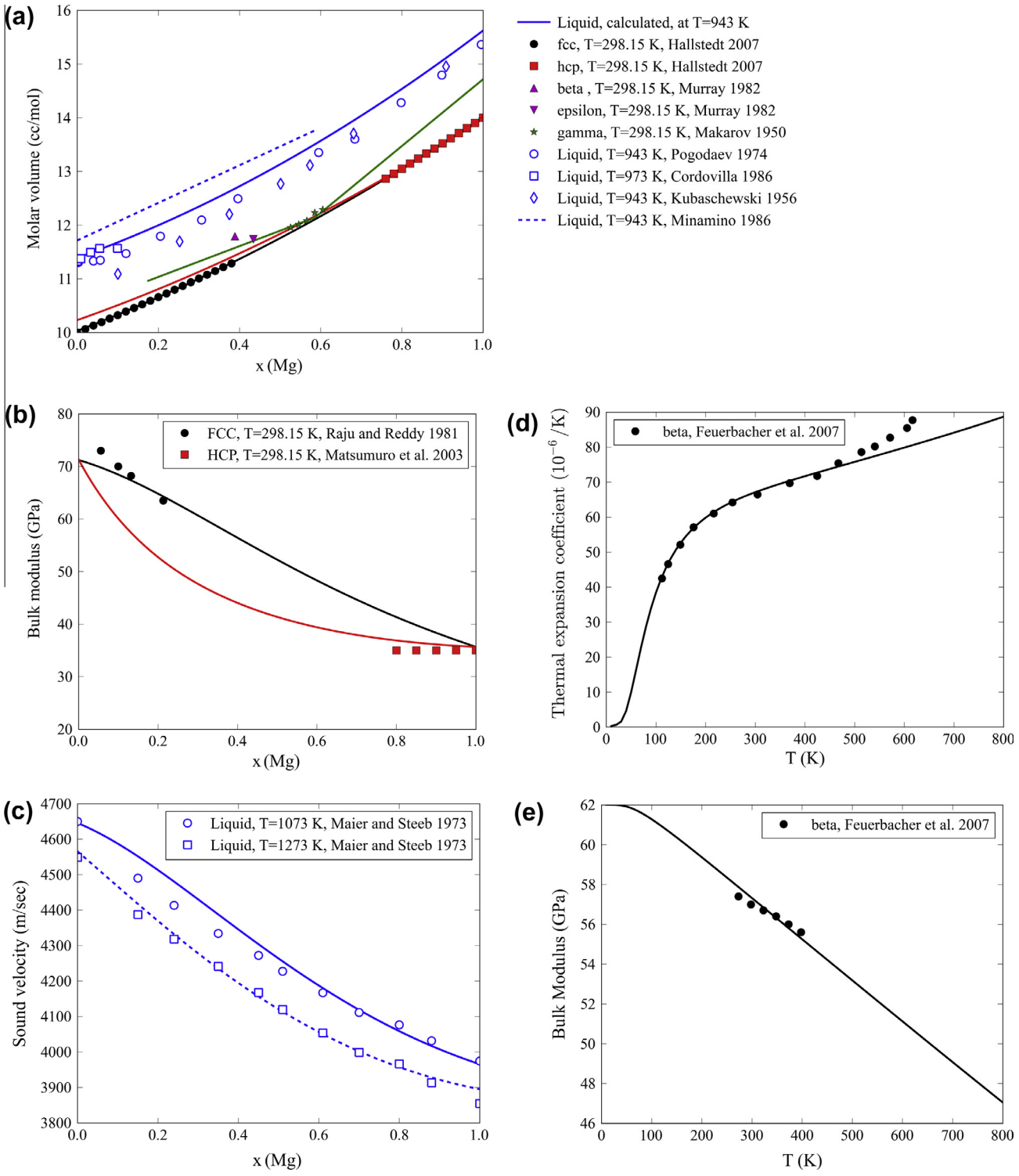

Fig. 6. Experimental thermophysical properties of Al–Mg alloys and compounds at ambient pressure and the corresponding fitted calculation. (a) Molar volume, (b) bulk modulus of solid solutions, (c) sound velocity in liquid alloys, (d) thermal expansion of the β phase, and (e) bulk modulus of the β phase.

pressure; for example, the Mg diffusion coefficient in the Al–4.06 at.% Mg at 732 K under normal atmospheric pressure is about 28 times that under 2.2 GPa [20]. The diffusion coefficients of Mg in the γ phase under normal atmospheric pressure are about 14 and 26 times that under 2.2 GPa and 3.3 GPa, respectively [5]. Hence, the diffusion of Mg atoms in the FCC solid solution and γ phase will be more difficult.

More evidence for the pronounced effect of pressure on diffusion in the present high pressure experiments arises from our microstructural analysis. While at ambient temperature, the composition of the γ phase was close to the ambient pressure equilibrium value, at high pressures it seems that the composition was frozen at higher temperature. The relatively rapid 20 K/s cooling rate in the present experiment might also contribute to the prevention of long-range diffusion. As evidence for this, one can notice that the concentration of Mg in the FCC in the current experiment was higher than the equilibrium values at high pressure measured by Minamino et al. Also, the phase content at 3 GPa is closest to

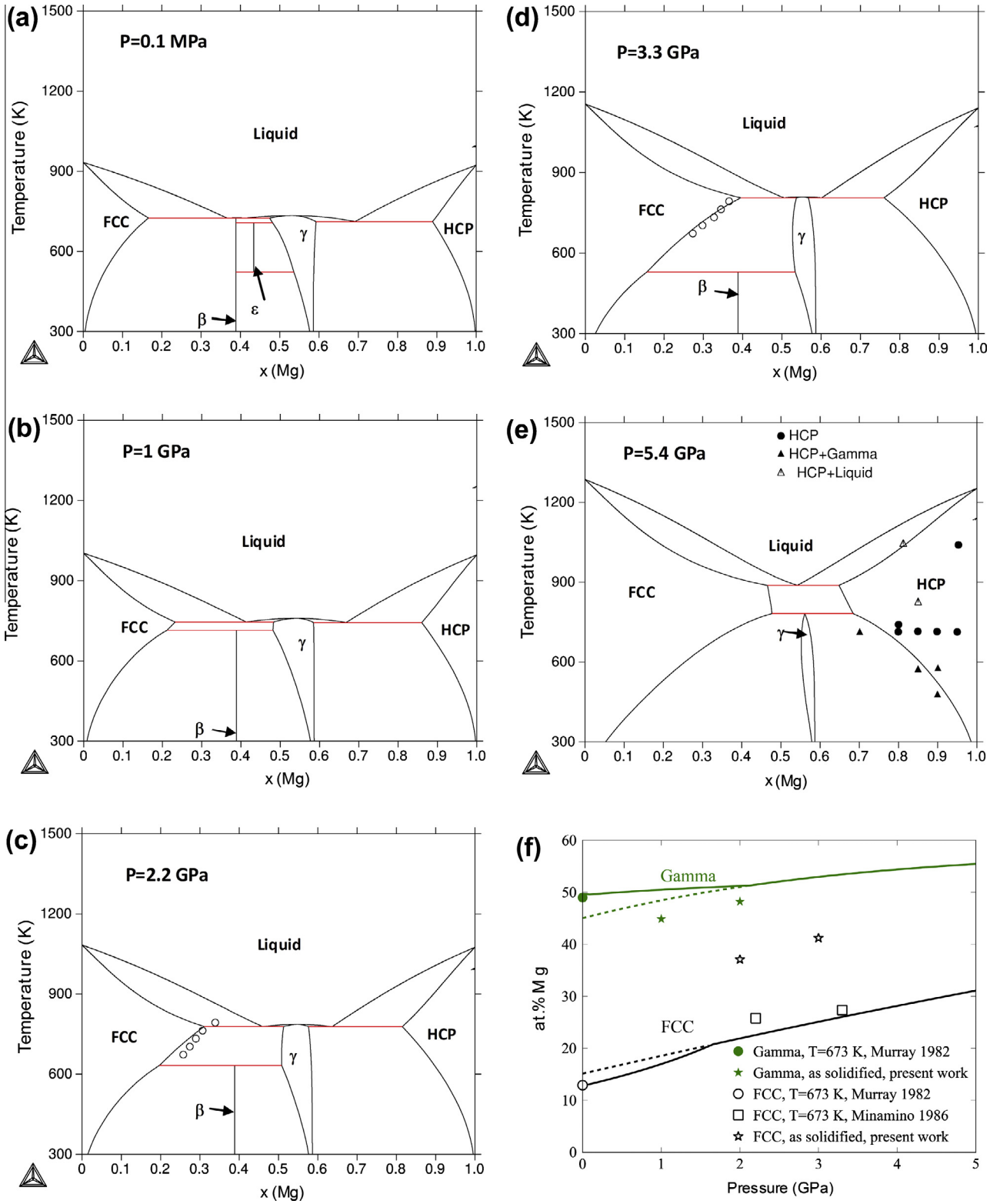

Fig. 7. Results of thermodynamic calculations and corresponding experimental results. (a) Al–Mg phase diagram at ambient pressure, for comparison with experiment see Zhong et al. [16]. (b) Calculated phase diagram at $P = 1$ GPa. (c) Calculated phase diagram at $P = 2.2$ GPa with experimental FCC solvus by Minamino et al. [5]. (d) Calculated phase diagram at $P = 3.3$ GPa with experimental FCC solvus by Minamino et al. [5]. (e) Calculated phase diagram at $P = 5.4$ GPa with experimental results by Matsumuro et al. [4]. (f) Calculated Mg content of the FCC and γ phases (on the Al-rich side) and corresponding results from Minamino et al. [5] and the present work. The ambient pressure results by Kurnakov et al. (cited by Murray [13]) are shown for reference. The dashed lines represent a metastable equilibrium calculation from which the β and ε phases are suspended.

Table 5
EOS model parameters of the pure elements, compounds, end members of the ordered γ phase and interaction parameters.

	N (−)[d]	V_0 (cc/mole atoms)	B_0 (GPa)	B_0' (−)	θ_0 (K)	γ_0 (−)	δ_0 (−)	b_0 (−)	δ_1 (−)	b_1 (−)
Fcc-Al	1	9.9	78	4.3	300	2.1	6	1	9	1
Hcp-Al	1	10.1	78	4.3	300	2.1	6	1	9	1
Liquid-Al[a]	1	10.55	70	4.5	300	2.1	6	1	15	1.1
Hcp-Mg	1	13.765	39.1	4.3	250	1.54	5	1	10	1
Fcc-Mg	1	13.8	39.1	4.3	250	1.54	5	1	10	1
Liquid-Mg	1	14.2	35.9	4.5	250	1.6	5	1	15	1
β-$Al_{140}Mg_{89}$	229	11.55	62	4.3	270	1.8	5	1	10	1
ε-$Al_{30}Mg_{23}$	53	11.72	55	4.3	250	1.8	5	1	10	1
γ-$Mg_5Al_{12}Al_{12}$[b]	29	11.1	60	4.3	270	1.8	5	1	10	1
γ-$Mg_5Al_{12}Mg_{12}$[b]	29	12.5	55	4.3	270	1.8	5	1	10	1
γ-$Mg_5Mg_{12}Al_{12}$[b]	29	12.03	55	4.3	270	1.8	5	1	10	1
γ-$Mg_5Mg_{12}Mg_{12}$[b]	29	14.5	39.1	4.3	270	1.54	5	1	10	1
Fcc-$Al_{0.5}Mg_{0.5}$[c]	1	11.584	58.5	4.3	–	–	–	–	–	–
Hcp-$Al_{0.5}Mg_{0.5}$[c]	1	11.664	45	4.3	–	–	–	–	–	–
Liquid-$Al_{0.5}Mg_{0.5}$[c]	1	12	60	2	–	–	–	–	–	–

[a] The parameters for liquid Al were altered to give better description at lower pressures (up to 10 GPa).
[b] The end members of the γ-phase ordered solid solution [16].
[c] For calculation of the interaction parameter according to Eqs. (12) and (4).
[d] (−) means dimensionless.

that calculated under the assumptions of partitionless solidification; that is, assuming very limited diffusion.

The reaction of α + γ → β requires long-range diffusion of Mg and is therefore suppressed in the high pressure solidification experiment. In contrast, the precipitation of β phase from supersaturated FCC during the solidification process, as in the Al–12Mg and Al–21.6Mg alloys at 1 GPa [6,18], should be easier, since it requires smaller diffusion distances.

5.2. The effect of high-pressure solidification on the mechanical properties of the alloy

Al–Mg intermetallic compounds are very brittle and have low mechanical properties at room temperature. The UTS of samples solidified under 3 GPa is greatly improved compared to those solidified under normal atmospheric pressure, mainly due to the formation of the large quantity of Al(Mg) solid solution with high Mg solubility. In the dilute Al(Mg) solid solution with Mg content less than 5 wt.%, the crucial mechanism of solute strengthening is that substitutional Mg atoms interact with mobile dislocations, e.g., edge and screw dislocations, leading to pinning of the dislocations and thus requiring greater applied stresses to move the dislocations [21,22]. Mechanical properties of Al(Mg) solid solution with high Mg solubility are rarely studied due to the difficult preparation method. In our recent studies, we have found that the tensile strength of solid solution first increases, and then decreases with increasing Mg solubility. Meanwhile, fractographic examination reveals that the fracture characteristic transforms from a dimple-like fracture to a combination of quasi-cleavage plus intergranular fracture with increasing Mg solubility [23].

Too high solubility of Mg in Al means that nearly half of the crystallographic positions in the Al unit cell are occupied by the Mg atoms, and the dislocation formed during the tensile process also contains about half Mg atoms. Thus, the Mg–Mg interaction and local clusters will play a very important role. For the Al(Mg) solid solution, the fracture is usually related to the nucleation and growth of voids [24]. During the tensile process of Al(Mg) solid solution with 41.6 at.% Mg, it is plausible to assume that the Mg atoms will segregate in the same given planes or regions of the Al lattice due to the stronger interaction. The voids are more easily formed due to the segregation process of Mg clusters, and the fracture occurs when there are enough voids to contact each other. Movement of the dislocation and fracture mechanisms in such a solid solution are very different from those in dilute Al(Mg) solid solution. Some behaviors may be similar to intermetallic compounds, and the sample exhibits typical characteristics of cleavage fracture (see Fig. 5b). This suggests that the formation of a solid solution with high Mg solubility is not an efficient way to improve the elongation of intermetallic compounds. Furthermore, the fracture is easy to propagate across the eutectic colonies distributed in the inter-dendritic region. Thus, the sample solidified under 3 GPa still exhibits a low elongation, although it has higher UTS.

6. Summary

Microstructure evolution, phase constitution, and tensile properties of Al–42.2Mg alloy composed of β-Al_3Mg_2 and γ-$Al_{12}Mg_{17}$ intermetallic compounds solidified under high pressures were investigated. A CALPHAD thermodynamic model of the Al–Mg system was extended to high pressures. Although the model could not fit some conflicting experimental results previously published in the literature, the agreement of the calculation with the present experiment is reasonable. One of the calculated results was that although the β phase is not expected to form directly from the melt at high pressure, it is still stable at lower temperature and may be expected to form by a peritectoid reaction. The fact that the β phase was not observed is explained by the decrease of diffusion coefficient under high pressure. The Al–42.2Mg alloy solidified under 3 GPa has remarkably improved ultimate tensile strength compared to the alloy solidified under normal atmospheric pressure. However, the elongation of a sample solidified under 3 GPa is still very low. In addition, the Al(Mg) solid solution with high Mg solubility exhibits the typical cleavage fracture characteristic, which is quite different from that of dilute Al(Mg) solid solution.

Acknowledgment

The authors gratefully acknowledge the financial support by National Natural Science Foundation of China under Grant No. 51171054.

Appendix A. The equation of state used in thermodynamic modeling and its parameters

The equation of state utilized in the present work was designed specifically for use in CALPHAD type calculations. It is consistent with explicit Gibbs energy models used in conventional CALPHAD databases, but unlike alternatives, it is constrained to physical

predictions of thermal expansion and heat capacity at high pressures. A full description and explanation of the EOS is given by Brosh et al. [25]. A short summary is given here for completeness.

In the present model, the molar volume entering Eq. (2) is divided into two parts[3]:

$$V(P,T) = V_c(P) + V_{th}(P,T) \tag{3}$$

a cold compression curve $V_c(P)$ and a "thermal volume" $V_{th}(P, T)$. The expression used here for the cold curve is:

$$V_c(P) = V_0 \cdot \left\{1 - \frac{3}{3B_0' - 1} + \frac{3}{3B_0' - 1} \cdot \left[1 + \frac{4}{9} \cdot (3B_0' - 1) \cdot \frac{P}{B_0}\right]^{1/4}\right\}^{-3} \tag{4}$$

where V_0, B_0 and B_0' are the molar volume, the bulk modulus, and its pressure derivative taken at ambient pressure and absolute zero temperature. Up to pressures of around $0.5 \cdot B_0$, the expression (4) gives results similar to the well-known UEOS [26,27] and it can be extended to extreme pressures by interpolating with the Thomas–Fermi model [26].

The temperature-dependent part $V_{th}(P, T)$ is derived from the following interpolation formula:

$$G(P,T) - G(P,T=0) = G^{QH}(P,T) - [G^{QH}(P_0,T) - G(P_0,T)] \cdot I(P) \tag{5}$$

where $G(P_0, T)$ is the Gibbs energy ambient pressure, taken from the ambient-pressure thermodynamic model, e.g., Zhong et al. [16]. $G^{QH}(P, T)$ is an approximation of the quasi-harmonic model:

$$G^{QH}(P,T) = 3NR \cdot T \cdot \ln[1 - \exp(-\theta/T)] \tag{6}$$

where R is the gas constant, N is the number of atoms per molecular formula, and θ is a pressure-dependent characteristic temperature that has a value θ_0 at ambient pressure and rises with temperature as:

$$\frac{d\ln\theta}{dP} = \frac{\gamma_0}{B_0} \cdot \{1 - \frac{1}{3b_0 - 1} + \frac{1}{3b_0 - 1} \cdot \left[1 + \frac{2}{3} \cdot (3b_0 - 1) \cdot (1 + \delta_0) \cdot \frac{P}{B_0}\right]^{1/2}\}^{-3} \tag{7}$$

where the model parameters γ_0 and δ_0 are related to the thermodynamically defined Gruneisen and Anderson-Gruneisen [28] parameters. b_0 is related to the pressure dependence of the Gruneisen parameter.

$I(P)$ is a monotonically decreasing interpolation function with the limiting values $I(0) = 1$, $I(\infty) = 0$. Its pressure dependence is given by:

$$\frac{dI}{dP} = -\frac{(1+\delta_1)}{B_0(1+b_1)} \cdot \exp\left[\frac{1}{b_1} - \frac{1}{b_1} \cdot \sqrt{1 + 2b_1 \cdot (1+\delta_1) \cdot \frac{P}{B_0}}\right] \tag{8}$$

with two additional model parameters b_1 and δ_1, related to the thermal expansion and the decrease of the bulk modulus at high temperatures.

An explicit expression for the "thermal volume" V_{th} is obtained by differentiating Eq. (3) with respect to pressure:

$$V_{th}(P) = 3NR \cdot \frac{\theta \cdot \exp(-\theta/T)}{1 - \exp(-\theta/T)} \cdot \frac{d\ln\theta}{dP} - [G^{QH}(P_0,T) - G(P_0,T)] \cdot \frac{dI}{dP} \tag{9}$$

[3] Here, the molar volume is written for a single composition so that the composition coordinate x is omitted.

The representation of the thermodynamic properties of phases in CALPHAD databases consists of two types of entities:

a. Unary descriptions of pure components, compounds, and "end-members" that may be pure components and real or hypothetical compounds. The model parameters V_0, B_0, B_0', γ_0, δ_0, b_0, δ_1, b_1 for the pure substances and solution end-members of in the Al–Mg system are given in Table 4.
b. Interaction parameters that embody the departure of the description of the solution from an ideal mixture of the end members. e.g., the cold component of the molar volume of a liquid or solid solution may be expressed by

$$V_c = x \cdot {}^0V_{c,Mg} + (1-x) \cdot {}^0V_{c,Al} + x \cdot (1-x) \cdot \Omega_0 \tag{10}$$

where x is the fraction of Mg atoms, ${}^0V_{c,Mg}$ and ${}^0V_{c,Al}$ are the "cold" molar volumes of pure Mg and Al, and Ω_0 is the zeroeth order Redlich–Kister interaction parameter for the molar volume.

For simplification, and in order to reduce the number of adjusted parameters, the interaction parameters were applied only to the cold compression and not to the thermal volume. i.e., as in our previous work [29], we assumed that for all solution phases:

$$V_{th} = x \cdot {}^0V_{th,Mg} + (1-x) \cdot {}^0V_{th,Al} \tag{11}$$

while the cold compression curves of solution phases are given by Eq. (10).

In order to make the interpretation of the zeroeth-order interaction parameter more intuitive, it was calculated in the following manner:

$$\Omega_0 = 4V_{c,Al_{0.5}Mg_{0.5}} - 2^0V_{c,Mg} - 2^0V_{c,Al} \tag{12}$$

where $V_{c,Al_{0.5}Mg_{0.5}}$ is the "cold" molar volume of an alloy having the composition $Al_{0.5}Mg_{0.5}$ described by Eq. (4). It can be checked by substitution of (12) in (10) that indeed at $x = 0.5$, the cold volume of the solution V_c is equal to $V_{c,Al_{0.5}Mg_{0.5}}$. The parameters V_0, B_0 and B_0' entering $V_{c,Al_{0.5}Mg_{0.5}}$ for the fcc, hcp, and liquid solution phases are given in Table 5.

References

[1] S. Samson, Acta Crystallogr. B 19 (1965) 401–413.
[2] P. Villars, L.D. Calvert, Pearson's Handbook of Crystallographic Data for Intermetallic Phases, second ed., ASM International, Ohio, 1985.
[3] J.R. Davis, ASM Handbook, Properties and Selection: Nonferrous Alloys and Special-Purpose Materials, vol. 02, second ed., ASM International, Ohio, 1990.
[4] A. Matsumuro, M. Futoshi, M. Masaya, K. Iwao, T. Yutaka, J. Soc. Mater. Sci. 52 (2003) 851–856.
[5] Y. Minamino, T. Yamane, T. MIyake, M. Koizumi, Y. Miyamoto, Mater. Sci. Technol. 2 (1986) 777–783.
[6] J.C. Jie, C.M. Zou, H.W. Wang, Z.J. Wei, Mater. Lett. 64 (2010) 869–871.
[7] J.C. Jie, C.M. Zou, H.W. Wang, B. Li, Z.J. Wei, Scripta Mater. 64 (2011) 588–591.
[8] H.L. Luo, C.C. Chao, P. Duwez, Trans. Metall. Soc. AIME 230 (1964) 1488–1490.
[9] S. Scudino, M. Sakaliyska, K.B. Surreddi, J. Eckert, J. Alloys Comp. 483 (2009) 2–7.
[10] A. Calka, W. Kaczmarek, J.S. Williams, J. Mater. Sci. 28 (1993) 15–18.
[11] M. Schoenitz, E.L. Dreizin, J. Mater. Res. 18 (2003) 1827–1836.
[12] J. Hanawalt, H. Rinn, L. Frevel, Anal. Chem. 10 (1938) 457–512.
[13] J.L. Murray, Bull. Alloy Phase Diagrams 3 (1982) 60–74.
[14] J.O. Andersson, T. Helander, L. Höglund, P.F. Shi, B. Sundman, Calphad 26 (2002) 273–312.
[15] N. Saunders, A.P. Miodownik, CALPHAD, A Comprehensive Guide, Pergamon Press, London, 1998.
[16] Y. Zhong, M. Yang, Z.-k. Liu, Calphad 29 (2005) 303–311.
[17] P. Liang, H.L. Su, P. Donnadieu, M.G. Harmelin, A. Quivy, P. Ochin, G. Effenberg, H.J. Seifert, et al., Z. Metallkd. 89 (1998) 536–540.
[18] J.C. Jie, C.M. Zou, H.W. Wang, Z.J. Wei, J. Alloys Comp. 506 (2010) L12–L15.
[19] M.V. Rooyen, P.F. Colijn, T.H.D. Keijser, E.J. Mittemeijer, J. Mater. Sci. 21 (1986) 2373–2384.
[20] K. Hisayuki, T. Yamane, H. Okubo, T. Okada, T. Takahashi, K. Hirao, Z. Metallkd. 90 (1999) 423–426.
[21] D. Olmsted, L. Hectorjr, W. Curtin, J. Mech. Phys. Solids 54 (2006) 1763–1788.
[22] A.S. Argon, Strengthening Mechanisms in Crystal Plasticity, Oxford University Press, London, 2008.
[23] J.C. Jie, C.M. Zou, H.W. Wang, B. Li, Z.J. Wei, J. Alloys Comp. 510 (2012) 11–14.

[24] T. Mukai, K. Higashi, S. Tanimura, Mater. Sci. Eng. A 176 (1994) 181–189.
[25] E. Brosh, G. Makov, R.Z. Shneck, Calphad 31 (2007) 173–185.
[26] E. Brosh, R.Z. Shneck, G. Makov, J. Phys. Chem. Solids 69 (2008) 1912–1922.
[27] P. Vinet, J.R. Smith, J.H. Rose, Phys. Rev. B 35 (1987) 1945–1953.
[28] O.L. Anderson, D.G. Isaak, J. Phys. Chem. Solids 54 (1993) 221–227.
[29] E. Brosh, G. Makov, R.Z. Shneck, Phys. Earth. Planet 172 (2009) 289–298.
[30] S. Scudino, S. Sperling, M. Sakaliyska, C. Thomas, M. Feuerbacher, K.B. Kim, H. Ehrenberg, J. Eckert, Acta Mater. 56 (2008) 1136–1143.
[31] X.G. Lu, M. Selleby, B. Sundman, Calphad 29 (2005) 68–89.
[32] D. Errandonea, Y. Meng, D. Husermann, T. Uchida, J. Phys.: Condens. Matter 15 (2003) 1277–1289.
[33] S. Ganeshan, S.L. Shang, Y. Wang, Z.K. Liu, Acta Mater. 57 (2009) 3876–3884.
[34] S.V. Stankus, R.A. Khairulin, Tsvetnye Metall. 9 (1990) 65–67.
[35] U. Maier, S. Steeb, Phys. Condens. Matter 17 (1973) 1–10.
[36] B. Hallstedt, Calphad 31 (2007) 292–302.
[37] W. Gasior, Z. Moser, J. Pstrus, J. Phase Equilib. 21 (2000) 167–171.
[38] V.K. Raju, P.J. Reddy, J. Phys. D: Appl. Phys. 14 (1981) 65–70.
[39] M. Feuerbacher, C. Thomas, J.P.A. Makongo, S. Hoffmann, W. Carrillo-Cabrera, R. Cardoso, Y. Grin, G. Kreiner, et al., Z. Kristallogr. 222 (2007) 259–288.
[40] E.S. Makarkov, Dokl. Akad. Nauk. SSSR 74 (1950) 935–938.
[41] H. Zhang, S.L. Shang, Y. Wang, A. Saengdeejing, L.Q. Chen, Z.K. Liu, Acta Mater. 58 (2010) 4012–4018.
[42] J. Wang, S.L. Shang, Y. Wang, Z.G. Mei, Y.F. Liang, Y. Du, Z.K. Liu, Calphad 35 (2011) 562–573.
[43] C. Garcia-Cordovilla, E. Louis, A. Pamies, J. Mater. Sci. 21 (1986) 2787–2792.
[44] O. Kubaschewski, J.A. Catterall, Thermochemical Data of Alloys, Pergamon Press, London, 1956.
[45] A.M. Pogodaev, E.E. Lukashenko, Nov. Teor. Tekhnol. Metall. Protsessov (1973) 83–86.